

# RECENT DEVELOPMENTS ON THE SLOW VISCOELASTIC FLOW PAST SPHERES AND BUBBLES

**B. Caswell**<sup>1</sup>, **O. Manero**<sup>2</sup> and **B. Mena**<sup>3</sup>

<sup>1</sup> Division of Engineering, Brown University, Providence, R.I. 02912

<sup>2</sup> Instituto de Investigaciones en Materiales, UNAM, Mexico, D.F.

<sup>3</sup> Instituto de Ingenieria, UNAM, Mexico, D.F.

## ABSTRACT

A review is presented covering the latest contributions to the slow viscoelastic flow past solid spheres and bubbles. The existing theoretical approaches are reviewed together with the available numerical methods. The proximity of container walls and its effect upon the motion of a sphere is also considered. Emphasis has been made on presenting recent experimental and numerical work intended to address some of the unresolved issues in this classic topic. Besides the so called "benchmark" problem of a viscoelastic fluid past a solid sphere centered on the axis of a long cylinder, this review addresses outstanding problems such as the wake behind the sphere, the negative wake, the depleted region effect as well as presenting some new results regarding the jump discontinuity in the velocity of rising bubbles.

**KEYWORDS:** Viscoelastic flow; Solid spheres, Bubbles, Numerical methods

---

## 1. INTRODUCTION

### 1.1 Historical Background

Non-Newtonian flow problems in the vicinity of the lower Newtonian regime have been solved by perturbation methods for about half a century. Even for the simple geometry of a sphere these calculations are formidable, and the range of their applicability is limited by the low order of the terms that can be reasonably calculated. Furthermore, the measurable properties of polymers typically vary as power laws of their arguments whereas the retarded motion expansions of the extra stress necessarily predict polynomial response. The limited range of applicability of these perturbations is offset by their universality since they involve only the coefficients of the "order fluids", and these can be obtained for any constitutive equation that exhibits regular response in the vicinity of the lower Newtonian regime, for example see chapter 6 of Bird et al. [1]. The perturbation analyses for "slightly viscoelastic fluids" of the early sixties, due to Leslie [2], Caswell et al [3], Giesekus [4] and, later, by Wagner [5] for fluid spheres, were followed by a stream of analytical and experimental papers on this subject.

The Reynolds number ( $R_e$ ) relating inertial to viscous forces, and the Weissenberg number ( $W_e$ ) representing the ratio of the characteristic relaxation time of the fluid to the convective time scale of the flow, are the small parameters of the problem. Other dimensionless groups are expressible as ratios of time constants, and may be suppressed for much of the discussion of the fluid dynamics. For a viscoelastic fluid, the inertialess ( $R_e = 0$ ) perturbation solutions predict the departure of the drag from Stokes law to be linear (Leal [6]) or quadratic in the Weissenberg number. The linear term vanishes with the fore-aft symmetry of the geometry relative to the flow direction, and this would appear to limit the interest since it does not predict substantial changes from the Newtonian solution.

On the other hand, the experimental problem offered rheologists an opportunity to perform apparently simple experiments measuring the drag on a falling sphere. Unfortunately it took some time and many erroneous papers (Turian et al [7], Karino et al [8] among others) to realize that experiments on falling spheres required a great deal of care. Many measurements were reported, before Cygan et al [9] brought attention to some of these experimental difficulties: surface effects, adsorption, homogeneity and stability of the fluid, flow visualization, wall effects, etc. to name a few.

In parallel, numerical solutions proliferated with a common factor that they were not valid for Weissenberg numbers beyond a certain value (i.e. more than two or three). One should bear in mind that large Weissenberg numbers, although possible, are not easily achieved experimentally without the introduction of inertia effects. An attempt to consider inertia using an Oseen type approximation (Mena et al [10]), showed a slight shifting of the streamlines in the flow direction but no major changes in the drag.

All of the above facts, together with the determination of many experimentalists to find "substantial differences" between Newtonian and non-Newtonian behaviour led to a number of experimentally questionable papers (Ultman et al [11], Cho et al [12,13]). It should be added, with due respect, that a great number of newcomers to the field, disregarded many of the pioneering theoretical analyses since they were "old" and were not easily accessible through the modern literature search methods; this inevitably led to numerous repetitions of previous results.

Several excellent review papers are available on the subject up to 1993. Specifically, the reviews of Walters and Tanner [14], the book by Chhabra [15] and an earlier review by Caswell [16] are obligatory reading for everyone working in the field. Therefore, this review paper will concentrate on the period after 1993 up to the present time.

Walters and Tanner [14] have reviewed much of the work, up to 1989, on the translation of a sphere in a viscoelastic medium. Their review compares the available experimental data for constant-viscosity elastic fluids and the large number of published numerical solutions. It has been pointed out that simulations for inelastic non-Newtonian fluid models that account for variable viscosity (usually shear-thinning) effects, on the one hand, and those carried out for constant viscosity elastic fluids, on the other hand, provide a methodology to analyze separately the effects

associated with viscoelasticity. Accordingly, comparison between experimental observation and numerical simulations is facilitated.

In this report, special emphasis has been made on presenting recent experimental and relevant numerical work intended to address some of the unresolved problems between experiments and numerical predictions. Furthermore, attention is also given to the outstanding problem related to the shortcomings of current constitutive equations.

The review is organized as follows: Section 2 re-examines some of the older perturbation analyses which, although applicable to a limited range of conditions, provide insight into some of the observable effects on particle motion, and are independent of particular constitutive assumptions. In section 3 we present the basic formulation of the drag on a sphere translating along the axis of a long tube. Attention is given to the variable viscosity inelastic fluids in section 4, while in section 5, the rheological behaviour of the translating sphere in a constant viscosity elastic (Boger) fluid is discussed. Section 6 deals with outstanding problems: the unsteady-state problem of the inception of motion of the sphere, the wake downstream of the sphere, the negative wake and the depleted layer effect. Finally, section 7 deals with some recent results for the dynamics of rising bubbles.

The creeping flow of a viscoelastic fluid past a solid sphere centred on the axis of a long cylinder has been identified as a "bench mark" problem for both numerical simulation and experimental investigation. The problem was arguably viewed as fundamentally important in non-Newtonian fluid mechanics (Walters and Tanner [14]). The non-viscometric character of the flow past a sphere suggests its use as a test of the predictions of rheological equations of state whose parameters have been fitted with rheometric data. Despite the development of a large body of numerical codes that simulate either transient or steady viscoelastic flows, the computed solutions often fail in direct quantitative comparisons with experimental measurements, Chhabra [15]. The most obvious factor involved in this discrepancy is the inadequacy of the constitutive models employed in the simulations.

## 2. PERTURBATION ANALYSES

The results of perturbation analysis are briefly reviewed here since they provide explicit form for the resistance to the flow past a body. The Reynolds number ( $Re$ ) relating inertial to viscous forces, and the Weissenberg number ( $We$ ) relating elastic to viscous forces are the small parameters for the problem in unbounded domains. Because of the uniformity of retarded motion expansions of the stress other dimensionless groups are expressible as ratios of time constants, and may be suppressed for the discussion of the dynamics of a particular fluid. Analytical solutions for creeping flow of viscoelastic fluids past a body are perturbations of the Newtonian solution. In an unbounded region the dimensionless velocity field is expanded in powers of  $We$ :

$$\mathbf{v} = \mathbf{v}_{st} + We \mathbf{v}_1 + We^2 \mathbf{v}_2 + \dots, \quad \dots\dots\dots(1)$$

with a corresponding expansion for the pressure field. The subscript 'st' stands for the solution of the linear Stokes problem. In plane flow and in axisymmetric flow expansion

(1) is often replaced by the equivalent expansion of the stream function  $\psi$ . Mena [10] evaluated the first and second non-Newtonian contributions  $\psi_1$  and  $\psi_2$  in a matched asymptotic expansion, and showed the streamline pattern to be slightly shifted in the downstream direction.

For symmetric bodies such as spheres expansion (1) predicts the departure from Stokes law to be  $O(W_e^2)$  in the corresponding expansion for the dimensionless drag (identical to the drag coefficient ratio):

$$D/D_{st} = 1 - (\lambda_s W_e)^2 + O(W_e^4) + \dots \quad \text{.....(2)}$$

where  $D_{st} = 6\pi a \eta_0 U$  is the Stokes drag for a sphere of radius  $a$  based on the zero shear-rate viscosity  $\eta_0$ , and  $U$  is the free stream velocity. The Weissenberg number  $W_e = U\lambda_s/a$  measures elastic effects as the ratio of a characteristic relaxation time of the fluid to the convective time scale  $a/U$  of the flow. For small departures from the lower Newtonian regime,  $W_e$  can be thought of as the ratio of a normal stress  $\lambda_s \eta_0 (U/a)^2$  to shear stress  $\eta_0 U/a$ . The time constant  $\lambda_s$  is a composite of the coefficients of the third order fluid.

The stream function for the flow may be expressed as:

$$\psi = \psi_{st} - O(W_e) \psi_1 + O(W_e^2) \psi_2 \dots \quad \text{.....(3)}$$

where  $\psi_{st}$  is the Newtonian stream function and  $\psi_1$  and  $\psi_2$  are the first and second contributions due to the non-Newtonian terms. The above expression shows a small shift in the streamline pattern in the downstream direction.

Results of this type were obtained independently by Leslie [2], Caswell et al [3], Giesekus [4] and for fluid spheres by Wagner [5]. A linear term appears for bodies without fore-aft symmetry in the flow direction, Leal [6]. Giesekus[4] appears to be the first to notice the universality of perturbation calculations, and thereby showed his results to be consistent with those of Leslie [2]. The most general results obtained so far are those of Wagner [5] for a non-Newtonian liquid drop moving in an immiscible non-Newtonian liquid. Special limiting cases of Wagner's results include the solid sphere and the bubble. Failure to appreciate universality has led to needless repetition of such calculations. The quadratic correction would appear to limit interest in the drag on a sphere at small  $W_e$  since it obviates substantial changes from the Newtonian case.

However, the explicit result for the drag and its inverse for the terminal velocity has been found to be useful for extrapolating experimental results in the vicinity of the lower Newtonian regime. Experimental confirmation of these theories has been given by Tanner [21], Broadbent et al [17], Manero et al [18], and several other authors.

A controversial paper by Ultman [11] simplified the Maxwell model (UCM) and the equation of motion with the Oseen linearisation. This linear system changes type from elliptic to hyperbolic when the ratio  $R_e/W_e$  is unity, and suggests the possibility of a discontinuity or front in the vorticity field. Although the analysis contains several inconsistencies, the most glaring of which is the use of the Oseen linearisation in the vicinity of the sphere, the possibility of a shift in the streamlines from downstream to upstream was shown at number  $W_e > 1$ . Although the analysis was incorrect, such a change has been found by several authors for high values of the Weissenberg number ( $W_e > 1$ ) (Zana et al [19], Tiefenbruck et al [20], Manero et al

[18]). The use of the UCM as a quantitative model has many pitfalls, in this case inertia combines to incorporate a change of type in the equations from elliptic to hyperbolic and allows for the appearance of discontinuities, leading to invalid solutions as shown by Tanner [21]. The fallacy here is to assume that the instantaneous modulus associated with the shear wave propagation is obtainable from accessible rheometric measurements.

The general conclusions regarding the slow flow of viscoelastic fluids past a sphere in an unbounded medium may be summarized as follows:

- a) Perturbation solutions are valid provided the small  $R_e$  and  $W_e$  conditions are met.
- b) For a viscoelastic fluid, the departure of the drag from the Newtonian purely viscous value follows a quadratic function of the Weissenberg number. Nevertheless, the quadratic departure appears to hold for values of the Weissenberg number much higher than the ones predicted by analytical solutions but in accordance to numerical predictions.
- c) For viscoelastic fluids in the low shear rate region and for constant viscosity elastic fluids, elastic effects are the predominant factor in the drag reduction and may not be considered negligible. For purely elastic fluids of the Boger type, the drag reduction appears to reach an asymptotic value at some critical value of the Weissenberg number, becoming independent of any further elastic effects. This is not the case if wall effects are present since a negative wake may appear.
- d) In the case of shear thinning viscoelastic fluids and for inelastic liquids at moderate and high values of the shear rate, shear-thinning properties are the dominant factor and are entirely responsible for the reduction in drag.
- e) Outside the creeping flow region, a simple knowledge of the viscosity as a function of shear rate is enough to provide a fairly accurate prediction of the drag on the sphere.
- f) The above conclusions are entirely valid for the slow flow past a cylinder.

### 3. RESISTANCE TO FLOW PAST A BODY

The resistance due to flow past a body is normally treated analytically as the exterior problem in an unbounded domain. For a given fluid the resistance is then an intrinsic property of the geometry of the body. Both experimental and numerical studies require finite domains, and this introduces the container geometry as a significant factor in understanding both the flow and the resistance. For a specified stream velocity  $\mathbf{U}$  the usual measure of resistance is the drag force function  $\mathbf{F}(\mathbf{U})$ , or its dimensionless version the drag coefficient. An alternative is to consider the force as specified and then  $\mathbf{U}(\mathbf{F})$  is the terminal velocity attained by the body under the action of  $\mathbf{F}$ . In steady flow, the drag and the terminal velocity functions are their respective algebraic inverses. For Newtonian fluids in the Stokes regime the inversion is a simple linear operation. In the non-linear regime the complexity of inversion suggests the desirability of presenting results as both the drag law and the terminal velocity

function. In most applications the force is imposed and the velocity is calculated or observed. Hence the terminal velocity function is likely to be the most useful measure of resistance. Analytically, the equations of motion together with velocity boundary conditions point to the specification of  $\mathbf{U}$ , and hence  $\mathbf{F}$  naturally becomes a dependent variable. However, a preference for the inverse problem, with  $\mathbf{F}$  specified and the terminal velocity as dependent variable, emerges from the analysis of the practical problem of separating out the effects of the container from the intrinsic resistance. The first order correction to the terminal velocities  $\mathbf{U}_\infty$ ,  $\mathbf{\Omega}_\infty$  of a body at a distance  $l$  from a boundary, and moving under the influence of external force  $\mathbf{F}$  and torque  $\mathbf{L}$  was shown by Caswell [23] to be:

$$\mathbf{U} = \mathbf{U}_\infty(\mathbf{F}, \mathbf{L}) + \mathbf{k} \cdot \mathbf{F} / 6\pi\eta_0 l + O(l^{-2}) \mathbf{\Omega} \psi = \mathbf{U}_\infty(\mathbf{F}, \mathbf{L}) + O(l^{-2}) . \quad \dots\dots\dots(4)$$

Here  $\mathbf{U}_\infty$  and  $\mathbf{\Omega}_\infty$  are the unbounded domain values of the translational and rotational velocities  $\mathbf{U}$  and  $\mathbf{\Omega}$ , respectively. The dimensionless wall-effect tensor  $\mathbf{k}$  is a property of the container geometry, and is determined from solutions of the Stokes system. For a body falling freely ( $\mathbf{L} = \mathbf{0}$ ) in a Newtonian fluid equation (4) was derived by Brenner [24] by inversion of the force formula obtained from the solution of the direct problem of Stokes flow past a body with the container boundary conditions satisfied by the method of reflections.

The representation of resistance as the drag coefficient as a function of Reynolds number is deeply ingrained in the fluid mechanics literature, but for non-Newtonian fluids it may be the least useful. Since for these materials inertia is often small or entirely negligible dimensionless groups containing the mass density would seem to be the least appropriate. Nonetheless the non-Newtonian resistance is still presented as a drag coefficient derived from numerical solutions of the inertialess equation of motion.

**4. VARIABLE VISCOSITY INELASTIC FLUIDS**

For a Newtonian fluid, the drag on a sphere of radius  $a$  translating longitudinally along the axis of a cylindrical container of radius  $R$  with a constant velocity  $U$  is given by :

$$D = 6\pi a \eta U K_N , \quad \dots\dots\dots(5)$$

where  $K_N$  represents the wall correction factor and has the following form:

$$K_N = \frac{l}{1 - f(a/R)} \quad \dots\dots\dots(6)$$

The function  $f(a/R)$  may be expressed in terms of the Faxen's series  $W(a/R)$  as:

$$f(a/R) = (a/R)W(a/R) = (a/R)[2.1044 - 2.088(a/R)^2 + \dots] \quad \dots\dots\dots(7)$$

In the limit of zero wall effects ( $R \rightarrow \infty$ ),  $f \rightarrow 0$  and equation (5) reduces to Stokes equation for the drag on a sphere translating in an infinite expanse of fluid:

$$D_{st} = 6\pi a \eta U_\infty . \quad \dots\dots\dots(8)$$

The relation between equations (5) and (8) is obtained by setting:

$$U_\infty = UK_N, \quad \dots\dots\dots(9)$$

where  $U_\infty$  represents the translating velocity that the sphere would have in an infinite medium.

In the case of a sphere translating in a non-Newtonian fluid, equation (5) may be generalised as follows:

$$D = 6\pi a \eta(\dot{\gamma})UK_u, \quad \dots\dots\dots(10)$$

where the apparent viscosity  $\eta$  is a function of the characteristic shear rate  $\dot{\gamma}$  and the wall correction factor  $K_u$  depends on the viscoelastic properties of the fluid. The above equation may be referred to the zero shear-rate viscosity  $\eta_0$ , so that equation (10) becomes:

$$D = 6\pi a \eta_0 U K. \quad \dots\dots\dots(11)$$

The following form for  $K_u$  is consistent with the shear-thinning inelastic approximation:

$$K_u = \frac{1}{1 - \frac{\eta(\dot{\gamma})}{\eta_0} f(a/R)}. \quad \dots\dots\dots(12)$$

As the shear rate tends to zero, the wall correction factor  $K_u$  approaches  $K_N$ , the correction factor for a Newtonian fluid (equation 6). Substitution of equation (12) into equation (10) yields:

$$K = \frac{\eta(\dot{\gamma})/\eta_0}{1 - \frac{\eta(\dot{\gamma})}{\eta_0} f(a/R)}. \quad \dots\dots\dots(13)$$

In the region where shear-thinning effects are predominant, at sufficiently high shear rates,  $\eta_0 \gg \eta(\dot{\gamma})$  and thus equation (13) becomes:

$$K = \frac{\eta(\dot{\gamma})}{\eta_0} = \frac{D}{D_{sto}}, \quad \dots\dots\dots(14)$$

where  $D_{sto}$  is the Stokes drag referred to the zero shear-rate viscosity. Equation (12) is similar in form to the expression proposed by Gu Dazhi and Tanner [24], i.e:

$$K_u = \frac{1}{1 - \alpha(n) \left(\frac{a}{R}\right)}, \quad \dots\dots\dots(15)$$

where  $\alpha(n)$  is a coefficient which depends on the power-law index  $n$ . Chhabra et al [25] reported extensive results on the translation of a sphere inside several cylindrical containers filled with inelastic shear thinning (power-law) fluids. The procedure to obtain the terminal velocity  $U_\infty$  from data of the measured terminal velocity  $U$  consisted in extrapolating linear plots of  $U$  versus  $a/R$  to  $a/R = 0$ . These authors proposed the following empirical correlation for  $K_u$  :

$$K_u = \frac{U_\infty}{U} = \frac{1}{1 - 1.6 \left( \frac{a}{R} \right)} \quad \dots\dots\dots(16)$$

The wall-effect coefficient in equation (16) is curiously close to 1.649 calculated by Kawaguchi [26], (see Brenner [23], p385) for the Newtonian case with a zero shear stress boundary condition on the cylinder wall (compare Faxen's 2.1044 for the zero wall velocity).

Numerical predictions of the wall correction factor  $K_u$  by Missirlis et al [27] using data from three of the fluids reported by Chhabra et al [25] show agreement with experimental data up to  $a/R = 0.43$ , validating the correlation shown in equation (16). Furthermore, it was shown that over most of the range of the power-law index, the value of the wall correction factor  $K_u$  diminishes with decreasing values of  $n$ , indicating that wall effects diminish with increasing fluid pseudoplasticity. This result is consistent with the analysis by Caswell [22]. In fact, the overall variation of  $K_u$  with power-law index shows a maximum for  $a/R$  ratios lower than 0.125. As the power-law index approaches zero, the drag coefficient  $K_u$  tends to a constant value independent of  $a/R$ .

Equations (12) or (13) have been verified experimentally. In fact, the onset of the shear-thinning dominated region in viscoelastic fluids may be found from the plot of the drag correction factor  $K_u$  versus Reynolds number  $R_e$ :

$$R_e = \frac{2a\rho U}{\eta(\dot{\gamma})} \quad \dots\dots\dots(17)$$

where the shear rate is defined as  $\dot{\gamma} = U/2a$ . In solutions of carbopol and polyacrylamide (an inelastic shear-thinning and a viscoelastic fluid, respectively) it was shown by Mena et al [28] that the shear-thinning behaviour is attained at lower  $R_e$  for the smallest  $a/R$  ratios than for the largest ones. For small  $a/R$  ratios, data points follow the pure inelastic correction equation (12) quite closely. For large  $a/R$  ratios, elastic effects play a dominating role at low Re numbers. Hence, application of equation (12) to viscoelastic data reveals the range where elastic effects are important and the region where the inelastic approximation given by equation (12) is adequate. Similarly, equation (14) has been verified by Mena et al [28] for Carbopol solutions, where data follows equation (14) very closely at high shear rates. At low rates deviations appear particularly for the larger spheres. This result is in agreement with predictions by Bush et al [29], which reveal that power-law approximations provide a good estimate of the drag force at moderate and high values of the effective shear rate.

Arigo and McKinley [30] presented data of a solution of polyacrylamide (2%) in 50-50% glycerol-water data for an aspect ratio  $a/R = 0.121$ . Excellent agreement was found between data and the purely shear-thinning correlation given in equation (13) at high Deborah numbers. In this case, the wall correction factor  $K$  is plotted with the shear-dependent Deborah number defined as:

$$D_e(\dot{\gamma}) = \lambda_I(\dot{\gamma})\dot{\gamma} = \frac{\psi_1(\dot{\gamma})}{2[\eta(\dot{\gamma}) - \eta_s]} \quad \dots\dots\dots(18)$$

where  $\lambda_1$  is the longest relaxation time,  $\psi_1$  is the first normal stress coefficient and  $\eta_s$  is the solvent viscosity.

Agreement with conclusions of Mena et al [28] has been also found in experiments with two highly shear-thinning fluids (1% Polyacrylamide in water and 2.5% Polyisobutylene in polybutene and decalin), reported by Navez et al [31]. In general terms, it was concluded in this work that shear thinning has a much stronger influence on the settling velocity than the fluid elasticity. The behaviour of the drag correction factor for wall effects (equation 11) as a function of the Weissenberg number, defined as:

$$W_e = \frac{\lambda U}{a} , \quad \dots\dots\dots(19)$$

is compared with that predicted for an inelastic generalized Newtonian model using the viscosity behaviour of the polymer solutions. Results of this comparison shows that predictions from the generalized Newtonian model are in agreement with the experimental results, which means that viscoelastic effects are much smaller than the drop in  $K$  due to shear thinning.

## 5. ELASTIC LIQUIDS

Experiments on the sphere translation in constant viscosity elastic fluids (Boger fluids) have been reported by Chhabra et al [25] and by Mena et al [28]. In solutions of polyacrylamide and corn syrup Chhabra et al observed a decrease in the drag coefficient ratio from the Stokes value of one to approximately 0.75, as the Weissenberg number increased from 0 to one. The drag coefficient is defined as follows:

$$C_D = \frac{D}{1/2\rho U_\infty^2 \pi a^2} , \quad \dots\dots\dots(20)$$

The Stokes drag coefficient,  $C_{Dst}$ , is obtained by substituting  $D_{st}$  from equation (8) into equation (20). For  $W_e$  larger than one, the drag ratio was found to be independent of the Weissenberg number.

Chmielewsky et al [32] found two different behaviours of the drag force depending upon the type of Boger fluid used in the experiments. Stokes law was obeyed for Weissenberg numbers up to 0.3 in the polyisobutylene-polybutene solutions (Type 2), then increased with  $W_e$ . In the polyacrylamide-corn syrup solution (Type 1), Stokes law was obeyed up to  $W_e = 0.1$ , but then decreased with increasing  $W_e$ . These results are in qualitative agreement with those of Tirtaatmadja et al [33]. These authors found increases up to  $K = 1.3$  for  $W_e = 2$ .

Jones et al [34] performed experiments on the two types of Boger fluids, and found that in the Type 1 solution the drag correction factor defined in equation (11) increases with Weissenberg number except near the value  $a/R = 0.5$ , where no increment was observed. In the limit of small aspect ratios, a drastic increase in the drag is observed ( $K = 3$  at  $W_e = 3$ ). In the Type 2 solution the drag correction factor increases with  $W_e$  and becomes independent of aspect ratio for  $a/R \leq 0.15$ . The

maximum in the drag correction is found when  $a/R = 0.2$  and decreases as  $a/R \rightarrow 0.5$ . The only observable reduction in the drag below the Newtonian value was found for aspect ratios  $a/R \rightarrow 1$ , but only at low  $W_e$ . For higher  $W_e$ , the drag increases again.

Further consideration was given by Degand and Walters [35] to include the case of a tightly fitting cylindrical container ( $a/R \sim 0.9$ ). In Type 1 solutions, data included experimental drag correction ratios (see equations 5 and 11)  $K/K_N$  plotted with the Weissenberg number obtained from both the falling sphere apparatus and the fixed sphere apparatus. The latter consisted of a pressure-driven flow past a stationary sphere in a cylindrical tube. Results show a Newtonian plateau for small  $W_e$  followed by a drag reduction, before another plateau is reached. Substantial drag enhancement as the extensional viscosity becomes dominant is observed at high  $W_e$  numbers.

Arigo et al [36] presented experimental data on the drag correction factor  $K$  as a function of the Weissenberg number using the Type 2 Boger fluid (0.31 wt % PIB/PB) for two aspect ratios (0.243 and 0.121). In the two cases, the same general behaviour is observed. For  $W_e < 1$  a small drag reduction is observed followed by an enhancement in the drag for larger  $W_e$  numbers, in agreement with Jones et al [34], Chmielewsky et al [32], Tirtaatmadja et al [33], and Becker et al [37]. The increase in the drag is more substantial for the larger spheres, and therefore the drag correction factor is dependent on the aspect ratio in this situation. For larger aspect ratios, the drag enhancement shows a decline, in agreement with results by Jones et al [34].

### **5.1 Theory on elastic liquids**

The C-R (Chilcott and Rallison [38]) dumbbell predictions show that, as  $W_e$  is increased, the drag coefficient is decreased from the Stokes value, reaching an asymptotic value at higher  $W_e$  numbers. This asymptotic limit, however, is not less than the Stokes value but depends upon the choice of the volume fraction of dumbbells and the extensibility parameter (ratio of the fully extended dumbbell to its equilibrium length). Chilcott and Rallison [38] found that for small values of the extensibility parameter (about 2 or 3) the drag coefficient would monotonically decrease from the Stokes value to some asymptotic value at high  $W_e$  numbers in agreement with experiments of Chhabra et al [25]. For much higher values of the extensibility parameter, the drag coefficient will also show a decrease from the Stokes value at low  $W_e$  numbers, but an increase at large  $W_e$ ; this increase reaching an asymptotic value. Hence, as  $W_e$  increases beyond one, the behaviour is governed by polymer extensibility. Furthermore, at high values of  $W_e$ , the drag is strongly dependent on the behaviour of the downstream wake. For large extensibilities, the dumbbells become highly deformed when  $W_e$  exceeds unity causing the drag coefficient to rise. For low extensibility, lesser deformation occurs downstream, and the drag does not rise. The comparison between Chilcott and Rallison and Chhabra et al analyses suggests that the PIB molecules can be stretched more by flow in polybutene than the PAA molecules in corn syrup. Intrinsic viscosity measurements (Kulicke and Haas [39] and McCarthy et al, [40]) indicate that corn syrup is a better solvent for PAA than the polybutene is for polyisobutylene. Hence, at equilibrium, PAA will be more extended relative to its contour length than will be the PIB.

Bush et al [41] examined the pressure flow past a sphere using DLV measurements in Type 1 Boger fluids and compared the measured axial velocity with finite element calculations using the PTT model. Very close to the rear stagnation point of the sphere, measurements showed an acceleration in the axial velocity exceeding that of a Newtonian fluid. However, further away from the stagnation region, the axial velocity field in the wake approached the free stream value more slowly than was observed in a Newtonian fluid. It was also found that large tube radii (smaller aspect ratio) resulted in a more gradual recovery of the axial fluid velocity to the far field value.

Arigo et al [36] have tested several constitutive equations: Phan-Thien-Tanner (PTT), Oldroyd B, Upper Convected Maxwell (UCM) and Chilcott-Rallison (CR) with multimode extensions to model the relaxation spectrum. Test fluids included a Type 2 Boger fluid. Results show a decrease in the drag of about 33% up to  $We = 2.2$ , considerably higher than the value found by Brown and McKinley [42]. Steep stress boundary layers develop around the sphere surface, with large stress gradients. A comparison of finite element simulations using the above models leads to several interesting conclusions: The Oldroyd-B model, which predicts an unbounded extensional viscosity in uniaxial elongation, shows a rapid decrease in  $K$  with increasing  $We$ , whereas the CR model captures the initial drag decrease but under-predicts the subsequent drag enhancement. The PTT model also under-predicts the drag, and is very sensitive to changes in the discrete viscoelastic spectrum of relaxation times.

Mitsoulis et al [43] have modelled the experimental results of Degand and Walters [35] using an integral constitutive equation of the K-BKZ type with a spectrum of relaxation times. For Type 2 Boger fluids, their predictions for the decrease in drag coefficient as a function of  $We$  appears reasonable up to  $We = 0.06$ . Experiments show an asymptotic decrease of 17%, from the Newtonian value at high  $We$ , which is not predicted in the numerical simulations. In shear-thinning elastic fluids, such as the test fluid S1, an enormous decrease in the drag is found (down to 0.1 of the Newtonian value); this may be attributed as 84% due to shear thinning and a further 16% due to viscoelasticity.

Yang and Khomami [44] made a comparative study between predictions from five constitutive equations and the experimental data of Arigo et al [36]. In this case, computations with the CR model showed that the drag decreases at low values of the extensibility parameter  $L$  ( $\approx 4$ ) while for high values, i.e.  $L = 12, 30$ , the drag decreases slightly and then monotonically increases. The multi-mode models of Verhoef et al [45] and Giesekus (see, for example, Larson, [46]) correctly predict the drag for  $We \leq 2$ , however, both models over-predict the drag for  $We$  larger than 2. The above models were also used to predict the drag for  $a/R = 0.243$ . For the latter geometry, the CR model with  $L = 30$  correctly predicts the measured drag up to  $We \approx 6$ . However, for larger values of  $We$  the model fails; this could be attributed to the fact that the model does not capture the strain hardening occurring at high  $We$ , as seen in the transient extensional viscosity of the test fluid. Comparison of the Verhoef et al and FENE-P (Bird, [1]) predictions indicate that the uniaxial extensional viscosity plays a significant role in determining the drag at  $We$  larger than one. In contrast with experimental observations reported for  $a/R = 0.12$ , multimode models under-predict

the drag. The tendency of the curve describing the drag coefficient is similar to the one describing the pressure contribution to the latter. Elastic effects tend to decrease the drag coefficient while viscous effects tend to increase the drag. Since the pressure at the surface is a sensitive function of the dissipative stresses, inclusion of these stresses in the constitutive model may indeed give rise to a larger drag coefficient. This is an important aspect that should be addressed by new constitutive models.

To summarize, it becomes apparent that none of the above models gives a quantitatively correct value of the drag, and that their ability to describe the experimental data cannot be ascertained by a simple examination of how well they describe the steady-state viscometric functions and the transient uniaxial extensional properties of the test fluid. As a general conclusion emerging from the above discussion, it is apparent that some important aspects of the underlying physics of the constitutive equations are missing.

## 6. UNSTEADY STATE

Early theoretical work on the transient motion of a sphere in an unbounded domain was performed by King and Waters [47] using the linear Jeffreys model coupled with the time-dependent form of the equations of motion for creeping flow. The analytic solution for the time-dependent velocity of the sphere showed velocity overshoots with damped oscillations about the ultimate steady-state settling velocity. The oscillations depend upon the elasticity number  $E$  representing the ratio of the  $W_e$  to  $R_e$  numbers. The solution can be expressed in the form:

$$\frac{U(t)}{U_\infty} = 1 + \frac{E}{\lambda_1 \omega} \sqrt{\left(1 - \frac{\lambda_2}{\lambda_1}\right)} \exp(-\varepsilon t) \sin(\omega t - \phi) \quad , \quad \dots\dots\dots(21)$$

where the damping rate  $\varepsilon$ , the oscillation frequency  $\omega$  and the phase angle  $\phi$  are given by:

$$\varepsilon = (1 + E\lambda_2 / \lambda_1) / 2\lambda_1 \quad , \quad \dots\dots\dots(22)$$

$$\omega = \left(E / \lambda_1^2 - \varepsilon^2\right)^{1/2} \quad , \quad \dots\dots\dots(23)$$

and

$$\phi = \arctan[\omega / (E / \lambda_1 - \varepsilon)] \quad . \quad \dots\dots\dots(24)$$

The elasticity number,  $E$ , is written as:

$$E = \frac{\lambda_1 \eta_0}{2a^2 \rho_f} \quad , \quad \dots\dots\dots(25)$$

and the ratio of the retardation time to the relaxation time is:

$$\beta = \frac{\lambda_2}{\lambda_1} = \frac{\eta_s}{\eta_0} \quad , \quad \dots\dots\dots(26)$$

where  $\rho_f$  is the fluid density and  $\eta_s$  is the solvent viscosity.

An integrated approach to solve the Oseen approximation, which yields solutions to both unsteady and steady problems, was presented by Mena and Caswell [10] for an Oldroyd-type of constitutive equation. The method used integral transform techniques, Laplace transform for the time and Fourier transform for the space variable. The use of Laplace transform gives the same solution as found by King and Waters [47] and later by Arigo and McKinley [30] for the unsteady (transient) flow past a sphere and the use of the Fourier transform gives the steady state solution for the sphere translating in an unbounded medium. The above solutions were obtained both for flow past a cylinder and for flow past a sphere, and the results were extended by matching them with the proper solution of the Stokes inertialess equation using asymptotic techniques. Approximate inversions of the Laplace transform had been obtained by Tanner [21] and by Thomas et al [48], and the exact inversion by King and Waters [47]. Later, an excellent paper by Arigo and McKinley [30] provided experimental results, which validate and extend the above theoretical predictions by considering wall effects.

Some analytical work using a second order fluid was presented by Ramkisoorn et al [49], while Bodart et al [50] and by Zheng et al [51], provided numerical simulations with quasi-linear models (the upper-convected Maxwell (UCM) and the Oldroyd B models) in the presence of walls. The work of Zheng et al using the UCM illustrates the strong effect that the aspect ratio  $a/R$  has upon the transients of the initial motion. Increasing the aspect ratio the frequency of the oscillations and the rate of damping increase while the amplitude of these oscillations decreases. Bodart et al [50] included inertia in their calculations and found that increasing the density of the spheres resulted in a decrease in the magnitude of the velocity overshoot of the sphere. Damped oscillations in the velocity of the sphere were predicted and a re-bounding effect was observed at some values of the model parameters. Increasing the aspect ratio led to an increase in the relative magnitude of the velocity overshoot with respect to the asymptotic settling velocity  $U_\infty$ .

Becker et al [37] presented experimental data of a Type 2 Boger fluid in a cylindrical container with an aspect ratio of 0.243. The analysis included inertia, for an Oldroyd B type equation in a single and multimode version. This work indicated that a spectrum of relaxation times is necessary to describe the initial transient acceleration of the sphere. This is valid even for low  $W_e$  when the applied stress is small and the steady-state motion corresponds to the zero shear-rate plateau region. The initial motion at short times and small strains remains unchanged and is well described by the linear viscoelastic limit. For the multimode models, the behaviour of the velocity following the overshoot appears to be dominated by the shortest of the time constants in the spectrum; this gives rise to a steeper slope and a faster decay to the asymptotic value found for the single-mode model. At longer times, the largest relaxation time dominates the long time asymptote towards steady-state. This results in a smaller slope than the one found for the single-mode model. The agreement with experimental data using multimode models is certainly better for high  $W_e$ . Predictions of the single mode model show the same qualitative behaviour as obtained in the experiments, but present a much larger overshoot followed by a monotonic decay to steady-state. The

multimode model does not capture the initial variation of the velocity (i.e. the initial slope  $dU/dt$ ) but gives a better description of the data.

An improvement of the above analysis was given by Rajagopalan et al [52], using the Type-2 Boger fluid over a wide range of Weissenberg numbers and aspect ratios ( $0.12 \leq a/R \leq 0.63$ ). In this case the combined effect of non-linear rheology and a spectrum of relaxation times was considered in the predictions. Once again, predictions fail to estimate accurately the initial slope  $dU/dt$  at the inception of flow around the sphere. In this region (short times) non-linear effects are not important and the behaviour is governed by inertia and the linear viscoelastic properties of the fluid. Experiments show that the velocity overshoot is insensitive to the aspect ratio, but due to the dependence of  $U$  with the latter, the relative overshoot actually increases as  $a/R$  decreases. Damped oscillations predicted by the models are not observed experimentally due to the large viscosity ratio. In addition, wall effects lower the settling velocity of the sphere and also increase the damping rate of the transient velocity overshoot arising from fluid elasticity.

Rajagopalan et al [52] mentioned that two conditions to obtain reasonable solutions to the flow problem are necessary. For low  $W_e$  numbers, a good description of the flow field in the transient shear flow in the gap between sphere and walls is necessary. At high  $W_e$ , a good description of the bounded extensional viscosity or the transient extensional viscosity of the fluid in the wake region near the rear stagnation point, is necessary.

For fluids that combine high elasticity and pronounced shear thinning (for example, polyacrylamide solutions), the initial transient motion of the sphere is governed by the linear viscoelastic properties of the fluid and the inertia of the sphere. The observed overshoot is larger than that found in Type 2 Boger fluids. Additionally, the sphere undergoes decaying oscillations about the final settling velocity, in qualitative agreement to the solution described by equation (21). In agreement with results for Boger fluids, the transient oscillations depend on the linear viscoelastic properties of the fluid, and constitutive non-linearities do not affect the initial motion of the sphere for times  $t \leq \lambda_1$ . Experimental observations reveal that the effect of increasing the aspect ratio is to decrease the frequency of the oscillations, while the rate of damping increases.

The inclusion of wall effects in equation (21) was described in Arigo and McKinley [30] by assuming that the velocity of the sphere is given at each instant by the Faxen solution. Equation (21) is then modified to account for wall effects as follows:

$$\frac{U(t)K_N}{U_\infty} = 1 + \frac{E_K}{\lambda_1 \omega_K} \sqrt{\left(1 - \frac{\lambda_2}{\lambda_1}\right)} \exp(-\varepsilon_K t) \sin(\omega_K t - \phi_K) , \quad \dots\dots\dots(27)$$

where:

$$E_K = EK_N(a/R) , \quad \dots\dots\dots(28)$$

$$\varepsilon_K = (1 + E_K \lambda_2 / \lambda_1) / 2\lambda_1 , \quad \dots\dots\dots(29)$$

$$\omega_K = \left( E_K / \lambda_l^2 - \varepsilon_K^2 \right)^{1/2}, \quad \dots\dots\dots(30)$$

and

$$\phi_K = \arctan[\omega_K / (E_K / \lambda_l - \varepsilon_K)]. \quad \dots\dots\dots(31)$$

Equation (27) shows that the effect of the walls is to increase the elasticity number. Hence, the frequency of oscillations decreases while the damping rate increases, in agreement with experiments. The analytic solution given by equation (21) provides only qualitative agreement with experiments. The use of a multimode formulation of the system of equations incorporating a relaxation times spectrum produces quantitative agreement with experiments in creep tests (Arigo and McKinley [30]).

### **6.1 The wake behind the sphere**

A great amount of numerical computations have pointed out that in axisymmetric flow past a rigid sphere the numerical solution normally breaks down at  $W_e$  numbers of order unity (Mendelsohn et al [53]) and Crochet et al [54]). As mentioned by Chilcott and Rallison [38], one likely source of this unwanted behaviour for an Oldroyd-type fluid, is the infinite polymer extensibility which gives rise to infinite stresses. The conditions under significant polymer deformation can be achieved for  $W_e$  numbers larger than unity and for sufficient time (larger than periods of order  $a/U$ ) allowing for high strains. These conditions can be met near stagnation points or in regions where the velocity is small. In rigid spheres, viscoelastic effects may be generated in the boundary layer near the surface of the sphere and also downstream of the sphere, in the region called "the wake" of the sphere. The uniaxial extensional flow at the rear of the sphere has a larger influence on polymer deformation than the biaxial extensional flow at the front of the sphere.

Experiments on flow birefringence past cylinders and spheres (Cressely and Hocquart [55] and Mead [56]) show two regions of different polymer response. A rapid initial extension in the neighbourhood of the stagnation point due to high velocity gradients gives rise to a high birefringence; this is followed by a gradual relaxation to equilibrium, leading to a slow decay of birefringence in the wake region. These experimental results have been compared with the predictions of the Chilcott and Rallison model [38].

Downstream along the axis of symmetry, the Chilcott and Rallison [38] model predicts polymer deformation which depends upon the  $W_e$  number and polymer extensibility. For high  $W_e$  numbers, a maximum in the polymer deformation is predicted as a function of axial distance from the sphere. Polymer deformation increases with  $W_e$  number. As the polymer extensibility parameter is increased, higher extensions of the polymer are achieved, thus reducing the polymer relaxation for a given extension. These predictions agree qualitatively with Chhabra et al [25] and Mena et al [28] results. The best value for the extensibility parameter that better fits the experimental data is quite small ( $\sim 3$ ). This explains the very thin and strong birefringent zone as observed in the experiments, thus suggesting that dumbbells can contribute sufficiently to the stress before they are stretched enough.

Numerical predictions of viscoelastic flow past a solid sphere using the upper-convected Maxwell (UCM) fluid for  $a/R = 0.5$  has been given special attention, particularly with regard to the accuracy of solutions at high  $W_e$  numbers. The major difficulty is to provide solutions to stress boundary layers on the sphere wall and to resolve the strong stress wake after the rear stagnation point as  $W_e$  increases. Various investigators have progressively increased the  $W_e$  number attainable for the UCM fluid up to 2.8 (Warichet and Legat [57], Luo [58], Arigo et al [36], Baaijens et al [59], Fan et al [60], Petera et al [61]). Fan et al [62] pointed out the problem that for sufficiently high values of the  $W_e$  number (i.e. 2.1) the positive definiteness of the Finger tensor is violated, thus concluding that the improvement of numerical algorithms is not the sole condition to obtain solutions at higher  $W_e$  numbers. In this regard, Sun et al [63] were able to obtain reasonable solutions up to  $W_e = 2.6$  without loss of positive definiteness using the adaptive viscoelastic stress splitting scheme. On the other hand, in the case of the Oldroyd-B model, Chauviere and Owens [64] found that the upper limiting  $W_e$  number for convergence is about 1.3, which is considerably lower than that of the UCM fluid.

Numerical solutions for  $W_e > 2$  sometimes present jumps in the shear and extensional stresses at the rear stagnation point. The appearance of a discontinuous shear stress can be traced to the complex boundary layer structure in the vicinity of the rear stagnation point (along the birefringence strand), where the axial normal stress and pressure have large axial gradients (Harlen [65]). In fact, for  $W_e > 2.15$ , the normal stress in the axial direction develops a maximum gradient with minimum boundary layer thickness. The three components of the stress near the rear stagnation point develop boundary layers with maximum stress gradients perpendicular to the flow direction.

The contour patterns of the axial normal stress ( $\tau_{zz}$ ) downstream of the rear stagnation point present lower values on the centreline than slightly off the centreline, depicting a thin boundary layer along the centreline that decreases sharply as one moves radially away. As  $W_e$  increases, this boundary layer becomes thinner, developing sharp stress gradients. According to Luo [58], the formation of the boundary layer derives from the high value of  $\tau_{zz}$  on the side surface of the sphere where the flow is a mixture of shear and elongation (strong flow region). The axial normal stress is convected downstream and attains its maximum slightly off the centre-line, while on the centre-line, the normal stress develops as a result of pure elongational flow starting from the rear stagnation region. The contours adjacent to the downstream pole of the sphere and associated with the stagnation point are compressed closer to the sphere thus developing a very intense stress gradient along the centreline. Resolution of this "birefringence strand" is the major difficulty in the numerical simulations (Lunsmann et al [66]).

In the case of the Oldroyd-B fluid, at the maximum attainable  $W_e$  number (1.3), positive definiteness is preserved. At this level of elasticity, jumps in the axial normal stress and shear stress occur near the rear stagnation point accompanied by strong oscillations, and they are restricted to a close vicinity of the stagnation region. Boundary layers are similar to those of the UCM fluid. The normal stress in the axial direction develops maximum gradients and the shear stress presents the smaller thickness. The near-singular behaviours of the UCM and Oldroyd-B fluids lie on the

infinitely extensible Gaussian chain, especially near the rear stagnation point where the fluid experiences a sudden transition from shearing to elongation.

In the case of the FENE model, for low extensibility of the dumbbell, the computations can exceed the limiting  $W_e$  number of the UCM fluid. On the other hand, for high extensibility, the resulting profiles exhibit similar stress boundary layers of the UCM fluid. The effect of finite extensibility is the reduction of the magnitude of the normal axial stress on the sphere wall and the normal radial stress in the birefringence strand.

With regard to calculations of the drag coefficient for the UCM fluid, agreement is found among most of seven different computing methods, which include those of Jin et al [67], Lunsmann et al [66], Khomami et al [68], Fan et al [69], Sun et al [63] and Baaijens et al [59] and Luo [58]. This agreement is excellent up to  $W_e$  around 1.4, but for higher values of  $W_e$  is less satisfactory, although the methods predict the same trend. The initial drag reduction for  $W_e$  around unity arises primarily from the transient viscoelastic response of the polymer in shear flow near the surface of the sphere and is followed by the development of the strong extensional wake or birefringent strand at higher  $W_e$  which causes a subsequent increase in the drag (Harlen [65]).

## **6.2 The negative wake**

The negative wake is a remarkable viscoelastic phenomenon consisting of an upward motion of the fluid behind the sphere, in the opposite direction to the falling sphere. Experiments on various fluids show that the existence of the negative wake is apparent in some polymers solutions, but in others a slow decay of the velocity downstream of the sphere (with no negative wake) has been observed. In polyethylene oxide solutions, Sigli et al [70] first observed a large region of negative velocity downstream of the sphere, and Bisgaard et al [71, 72] observed a slow decay of the downstream velocity followed by a negative wake in polyacrylamide solutions. In these solutions, the presence of the negative wake was also confirmed by Arigo and McKinley [73] and, in experiments with shear-thinning fluids, Maalouf and Sigli [74] also found negative wakes. Quite different behaviour is exhibited by the Boger fluids. Arigo et al [36] observed a slow decay (slower than that of a Newtonian fluid) of the velocity downstream (with no negative wake) in Type 2 Boger fluids, but Bush [75] reported the presence and absence of the negative wake in Type 1 Boger fluids, depending on the ratio of water to corn syrup. It appears that shear thinning is not the sole ingredient necessary for negative wakes, but a combination of shear-thinning and the extensional properties of the fluid. Furthermore, all fluids that show negative wakes are concentrated solutions where entanglement effects are important. Another experimental fact is that the negative wake is a non-linear effect present at large strains long after the transient oscillations associated with linear viscoelasticity and fluid inertia have decayed (Arigo and McKinley [73]).

Numerical calculations indicate that the formation of a negative wake is related to situations where elasticity dominates simultaneously to the presence of a small increase in the elongational viscosity. Hence, this phenomenon is closely connected to

the extensional properties of the constitutive model, in particular with the extensibility parameter of the FENE model.

Harlen [76] has performed a comparative study of predictions of the wake patterns produced downstream the sphere using three different models (FENE-CR, FENE-P and Giesekus). The FENE-CR (Chilcott and Rallison model) predicts negative wakes for small values of the extensibility parameter (which scales with the Trouton ratio) and extended wakes as the extensibility parameter increases. Satrape et al [77] also found negative wakes for small values of the extensibility parameter. The effect of the  $W_e$  number on the downstream velocity is to increase the magnitude of the reverse flow but the stagnation region remains fixed (Satrape et al [77], Harlen et al [78]). In summary, for small values of the extensibility parameter (or Trouton ratio), corresponding to a small increase in the extensional viscosity, the magnitudes of the tensile stresses are strongly reduced and become comparable to the magnitude of the shear stresses. This suggests that the rapid radial variations in the shear stress dominate the slow decay of the small extensional stresses giving rise to negative wakes. Computations show that under these circumstances, the stagnation region moves towards the sphere with increasing  $W_e$  numbers, in agreement with the experiments of Sigli et al [70].

Harlen's [76] calculations also show that the magnitude of the reverse flow increases with the aspect ratio  $a/R$  and the negative wake disappears for values lower than  $a/R = 0.2$ , in agreement with results from Satrape et al [77] and Sigli et al [70]. Moreover, the position of the minimum in the velocity is a function of the  $W_e$  number and shifts farther downstream as  $W_e$  increases. An interesting observation is that in the limit of very low extensibility, the flow behaviour is that of an entangled system at strain rates of order of the inverse reptation time. In this limit, the stress arises from the orientation distributions of tube segments that relax by reptation. In addition, Harlen has proposed that the negative wake may be caused by an elastic recoil of the shear stress in the region outside the strand, which pulls the liquid in the strand away from the sphere. Hence, the velocity perturbation depends on the relative magnitude of the elongational tensile stresses and the shearing stresses in the wake.

### **6.3 The depleted region effect**

In highly elastic fluids, the terminal velocity of the falling sphere can be strongly dependent on the time interval between the dropping of successive balls. Experiments by Bisgaard [72], Cho et al [79], Ambeskar and Mashelkar [80], Jones et al [34] and Degand and Walters [35] show that this effect is apparent over a time scale much larger than the rheological relaxation time scale of the solutions, and sometimes lasts several hours. In Type 2 Boger liquids this phenomenon has been observed when the time interval between successive drops approaches 15 min. Results by Jones et al [34] show that the terminal velocity increases on successive drops before reaching an asymptote after five drops, and a period of 24 h is required before full recovery of the solutions. With other test fluids, Type 1 Boger fluid and the fluid S1 (2.5% polyisobutylene in 19/20 parts decalin/polybutene oil) the depleted region effect was absent.

The basic explanation for this effect is still absent and the problem remains unresolved, although several particular explanations have been given. As the sphere displaces fluid during its motion, it breaks the high molecular weight polymer network, inducing extended chain configurations that relax with constrained Brownian motion over a long period of time. A change in the refractive index of the solution is sometimes observed after the sphere has stopped its downward motion.

## 7. VISCOELASTIC FLOW PAST A BUBBLE

This section deals with observations of a bubble that rises in a container filled with a viscoelastic fluid. Flow past a bubble is of interest because it might shed light on the possible causes of the negative wake phenomenon. Bisgaard [72] and Hassager [81] both reported large negative wakes for bubbles and for solid spheres, and a strong sensitivity of the drag on a bubble to the flow field downstream. The stress concentration at the rear stagnation point produces a deformation of the bubble from a spherical shape with a cusp or knife-edge form to the rear, and this change in shape may have a marked effect on the drag by changing the structure of the wake.

Experiments by Astarita et al [82], Zana and Leal [83] and Leal et al [84] show a discontinuous increase in the terminal velocity of a rising bubble in a non-Newtonian fluid at near zero  $Re$  number. This discontinuity occurs at a critical bubble radius (or critical  $We$  number). The change in the shape of the bubble near the rear stagnation point into a concave cusp replaces the extensional flow to the rear by a shearing region, which reduces the drag, and hence the terminal velocity of the bubble rises drastically. The shape of the surface near the tip requires a sort of converging flow, which causes the velocity to rise downstream of the tip. This may be a contributing factor to the appearance of the negative wake observed experimentally (Chilcott and Rallison [38]). Liu et al [85] also suggested that the appearance of the jump resulted from a transition in shape and the appearance of a cusp at the rear of the bubble. Rodrigue et al [86] presented experimental data, which show that the cusp formation may be caused, in part, by wall effects. These authors gather data from various studies on bubble dynamics (Rodrigue et al [87], Leal et al [84], Liu et al [85]) and show that the critical capillary number, defined as:

$$Ca = \frac{\eta_0 U}{\sigma} \quad , \quad \dots\dots\dots(32)$$

where  $\sigma$  is the interfacial tension, is of order one at the discontinuity. Although in a strict sense the critical capillary number by itself cannot be used to determine the occurrence of the jump, nevertheless it could indicate the region in the velocity- $We$  number curve where the discontinuity is likely to occur.

Recent experiments by Herrera et al [88] on Polyacrylamide solutions confirm the observations presented in the mentioned papers. Moreover, experiments performed using a solution of an associative polymer bearing n-alkyl hydrophobes, the so-called "HASE" polymers, show that at the discontinuity point, the cusp at the rear of the bubble evolves into an elongated shape of several bubble radii in length, quite similar to having a slender body downstream of the bubble. Since these polymers are surface-active macromolecules, the interfacial tension is diminished substantially, to values

smaller to that of the water. This in turn increases the value of the critical capillary number for a given stress. These results suggest that the major contribution to the bubble deformation near the rear stagnation point is due to the uniaxially extensional flow dominated region causing the deformation of the molecules, in agreement with conclusions by Noh et al [89]. In that respect, it would be reasonable to define the capillary number in equation (29) in terms of the local extensional stress. Additional support to these conclusions are the results of recent experiments on shear-thinning inelastic fluids (Herrera et al [88]) in which no change in shape is observed, and hence the discontinuity is absent.

More recently, Zenit et al [90] have examined separately the effect of shear thinning and elasticity upon the flow past bubbles. Several interesting conclusions are reached from the experiments:

- For a purely elastic, constant viscosity Boger type fluid, the evolution of the bubble shape varies with bubble volume but the jump discontinuity in bubble velocity does not appear for a critical volume. The bubble shape changes from spherical to an elongated shape as the volume increases. A negative wake may or may not be present at this stage. This is shown in Figure 1.
- For an inelastic shear thinning fluid, the evolution of the bubble shape varies from a spherical geometry to a cap form as the volume of the bubble is increased. Nevertheless, again, no jump discontinuity was observed but drag reduction is always present. Figure 2.
- For a viscoelastic fluid, the jump discontinuity appears at a critical volume, together with the appearance of a negative wake and a transition in shape may be observed to a knife-edge tail. This is shown in Figure 3.
- A curious phenomenon occurring for both viscoelastic and purely elastic fluids, is the appearance of the knife-edge tail as seen in Figure 4. Under these conditions, the bubble rotates around its vertical axis as it moves towards the surface.

If the Stokes drag coefficient for the bubble is defined from the usual gravity balance as:

$$C_D = \frac{4}{3} \frac{d_b}{U_b^2} g \quad , \quad \dots\dots\dots(33)$$

and the Reynolds number is defined as:

$$R_e = \frac{U_b \rho_f d_b}{\eta_0} \quad , \quad \dots\dots\dots(34)$$

the experimental data may be plotted for the various types of fluids. This is shown in Figure 5.

For viscoelastic fluids at various concentrations of polyacrylamide in water and water-glycerol solutions, the drag coefficient is always below the Newtonian Stokes value as expected. Also, at a critical volume of the bubble, a jump discontinuity in the velocity appears, thus reducing the total drag even further.

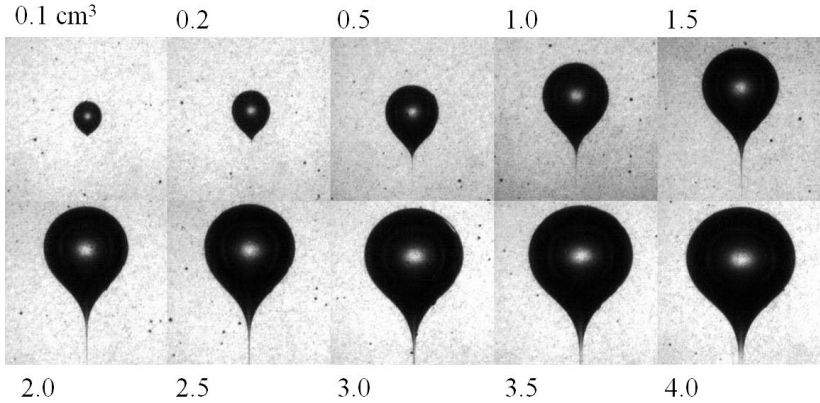


**Figure 1:** Evolution of the bubble shape with bubble volume for a purely elastic, constant viscosity Boger type fluid. The bubble shape changes from spherical to an elongated shape as the volume increases. A negative wake may or may not be present at this stage.

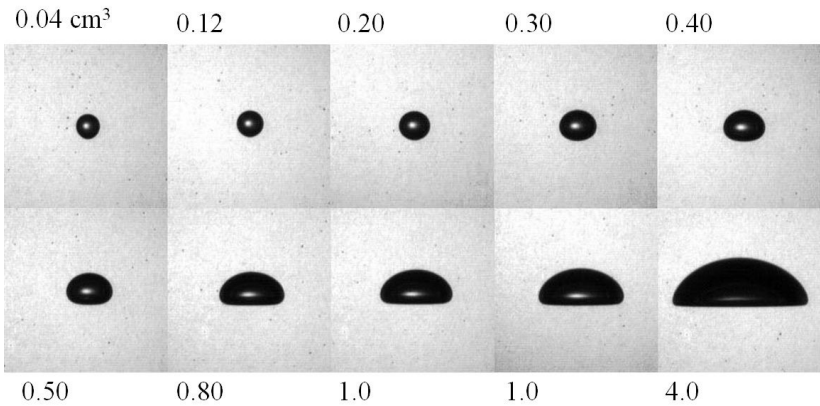


**Figure 2:** Evolution of the bubble shape for an inelastic shear thinning fluid. Variation from a spherical geometry to a cap form as the volume of the bubble is increased. No jump discontinuity was observed but drag reduction is always present.

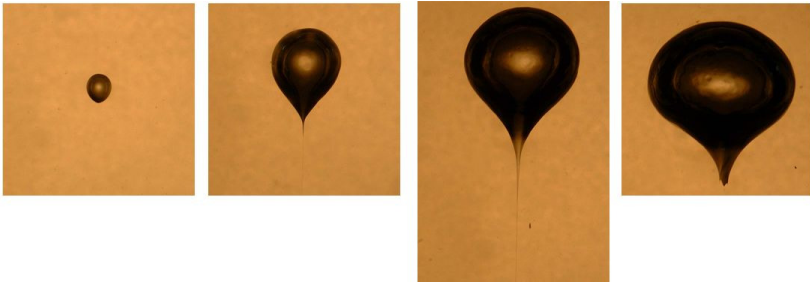
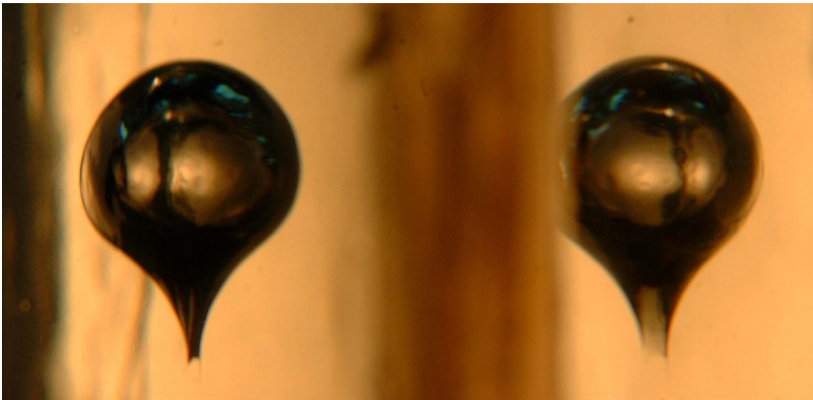


**Figure 3:** For a viscoelastic fluid, the jump discontinuity appears at a critical volume, together with the appearance of a negative wake and a transition in shape may be observed to a knife-edge tail.



Top view:



**Figure 4:** A curious phenomenon occurring for both viscoelastic and purely elastic fluids, is the appearance of the knife edge tail. Under these conditions, the bubble rotates around its vertical axis as it moves towards the surface.

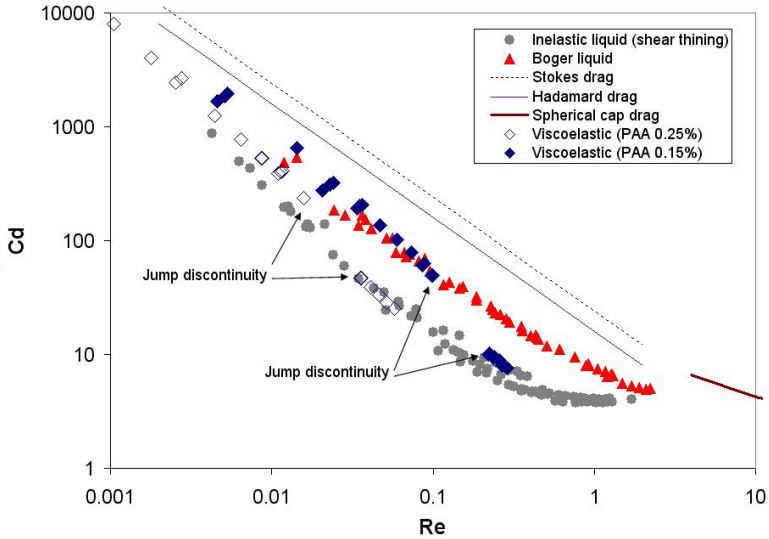


**Figure 5:** Experimental data plotted for all the various types of fluids.

In the case of constant viscosity elastic liquids of the Boger type, the drag coefficient is below the Stokes value for all the Boger fluids considered. It is noticeable that the amount of elasticity (polymer concentration) in the fluid does not appear to alter the amount of the drag departure.

For inelastic shear thinning liquids, the drag is always below the Stokes value independently of the fluid viscosity. In this case the drag departure is due only to shear thinning effects. No discontinuity in the velocity appears and there is no negative wake.

A curious result that emerges from the above experimental data is that both the Boger type fluids and the inelastic fluids show a drag reduction when compared with the Stokes drag but the combined effects of elasticity and shear thinning properties are not really distinguishable from the purely elastic effects upon the drag. The only explanation offered by the authors, is that this is due partly to the shape of the bubble and, most of all, due to elongational effects in the tail of the bubble which result in an increase in the total drag due to elasticity which tends to overshadow the shear thinning effects. This ceases to be true when the jump discontinuity appears at a critical volume; in this case, the bubble rising in a viscoelastic fluid presents a substantial drag decrease attributable to the change in shape; also, a negative wake appears which probably does not contribute to the increase in velocity but drastically affects the flow conditions at the far field.

## ACKNOWLEDGEMENTS

The authors acknowledge the support received from CONACYT, project NC-204 and UNAM- PAPIIT IN108901. Special thanks are due to R. Zenit for allowing us to include some of his latest results.

## REFERENCES

1. Bird R B, Armstrong R C, and Hassager O, *Dynamics of Polymeric Liquids, Fluid Mech. Vol. 1*, Wiley, New York, (1987).
2. Leslie F M, *Quart. J. Appl. Math.*, 14 (1961) 36.
3. Caswell B and Schwarz, *J. Fluid Mech.*, 13 (1962) 417.
4. Giesekus H, *Rheol. Acta*, 3 (1963) 59.
5. Wagner M and Slattery J C, *AICHE J.*, 17 (1971) 1198.
6. Leal LG, *J. Fluid. Mech.*, 69 (1975) 305.
7. Turian R M, *AICHE J.*, 13 (1967) 999.
8. Karino I, Konno H, Ozeki E and Egawa S, *Proc. Soc. Chem. Engrs. Japan*, (1972).
9. Cygan D A and Caswell B, *Trans. Soc. Rheol.*, 15 (1971) 663.
10. Mena B and Caswell B, *Chem. Eng. J.*, 8 (1974) 125.
11. Ultman J S and Denn M, *Chem. Eng. J.*, 2 (1971) 81.
12. Cho Y I and Hartnett J P, *Lett. Heat Mass Transf.*, 6 (1979) 335.
13. Cho Y I, Hartnett J P and Kuack E Y, *Chem. Eng. Commun.*, 6 (1980) 141.
14. Walters K and Tanner R I, "The motion of a sphere through an elastic fluid", in "Transport Processes in Bubbles, Drops, and Particles", (Editors: Chhabra R P and De Kee D), Hemisphere Pub., (1992).
15. Chhabra R P, in "Bubbles, Drops, and Particles in non-Newtonian Fluids", CRC Press, Boca Raton, Florida, (1993).
16. Caswell B, *ASME AMD*, 22 (1977) 19.
17. Broadbent J M and Mena B, *Chem. Eng. J.*, 8 (1974) 11.
18. Manero O and Mena B, *J. Non-Newtonian Fluid Mech.*, 9 (1981) 379.
19. Zana E, Tiefenbruck G and Leal LG, *Rheol. Acta*, 14 (1975) 891.
20. Tiefenbruck, G and Leal L G, *J. Non-Newtonian Fluid Mech.*, 10 (1982) 115.
21. Tanner R I, *Z.A.M.P. XIII*, 6 (1962).
22. Caswell B, *Chem. Eng. Sci.*, 25 (1970) 1167-1176.
23. Happel J and Brenner H, *Low Reynolds Number Hydrodynamics*, Prentice Hall, N.J. (1965).

24. Gu Dazhi and Tanner R I, *J. Non-Newtonian Fluid Mech.*, 17 (1985) 1-12.
25. Chhabra R P, Uhlherr P H T and Boger D V, *J. Non-Newtonian Fluid Mech.*, 6 (1980) 187-199.
26. Kawaguti M, *J. Phys. Soc. Japan*, 10 (1955) 694.
27. Missirlis K A, Assimakopoulos D, Mitsoulis E, and Chhabra R P, *J. Non-Newtonian Fluid Mech.*, 96 (2001) 459-471.
28. Mena B, Manero O, and Leal L G, *J. Non-Newtonian Fluid Mech.*, 26 (1987) 247-275.
29. Bush, M B and Phan-Thien N, *J. Non-Newtonian Fluid Mech.*, 16 (1984) 303-313.
30. Arigo, M T and McKinley G H, *J. Rheol.*, 41(1997) 103-128.
31. Navez, V and Walters K, *J. Non-Newtonian Fluid Mech.*, 67 (1996) 325-334.
32. Chmielewsky C, Nichols K L and Jarayaman K., *J. Non-Newtonian Fluid Mech.*, 35 (1990) 37-49.
33. Tirtaatmadja V, Uhlherr P H T and Sridhar T, *J. Non-Newtonian Fluid Mech.*, 35 (1990) 327.
34. Jones W M, Price A H, and Walters K, *J. Non-Newtonian Fluid Mech.*, 53 (1994) 175-196.
35. Degand, E. and Walters, K., *J. Non-Newtonian Fluid Mech.*, 57 (1995) 103-115.
36. Arigo M T, Rajagopalan D, Shapley N and McKinley G H, *J. Non-Newtonian Fluid Mech.*, 60 (1995) 225-257.
37. Becker L E, McKinley G H, Rasmussen H K and Hassager O, *J. Rheol.*, 38 (1994) 377-403.
38. Chilcott M D and Rallison J M, *J. Non-Newtonian Fluid Mech.*, 29 (1988) 381-342.
39. Kulicke W M and Haas R, *Ind. Eng. Chem. Fundam.*, 23 (1984) 308.
40. McCarthy K J, Burkhardt C W and Parazak D P, *J. Appl. Polym. Sci.*, 33 (1987) 1699.
41. Bush M B, *J. Non-Newtonian Fluid Mech.*, 49 (1993) 1093.
42. Brown R A and McKinley G H, *J. Non-Newtonian Fluid Mech.*, 52 (1994) 407-413.
43. Mitsoulis E, *J. Non-Newtonian Fluid Mech.*, 74 (1998) 263-283.
44. Yang B and Khomami B, *J. Non-Newtonian Fluid Mech.*, 82 (1999) 429-452.
45. Verhoef M R J, van den Brule B H A A and Hulsen M A, *J. Non-Newtonian Fluid Mech.*, 80 (1999) 155-182.
46. Larson R G, "Constitutive Equations for Polymer Melts and Solutions",

Butterworths, Boston, (1998).

47. King M J and Waters N D, *J. Phys. D: Appl. Phys.*, 5 (1972) 141-150.
48. Thomas R.H. and Walters K, *Rheol. Acta*, 5 (1966) 23.
49. Ramkissoon H and Shifang H, *Int. J. Eng. Sci.*, 31 (1993) 19-26.
50. Bodart C and Crochet M J, *J. Non-Newtonian Fluid Mech.*, 54 (1994) 303-329.
51. Zheng R and Phan-Thien N, *Rheol. Acta*, 31 (1992) 323.
52. Rajagopalan D, Arigo M T and McKinley G H, *J. Non-Newtonian Fluid Mech.*, 65 (1996) 17-46.
53. Mendelshon M A, Yeh P-W, Brown R A and Armstrong J, *J. Non-Newtonian Fluid Mech.*, 10 (1982) 31-54.
54. Crochet M J, Davies A R, and Walters K, "Numerical Simulation of Non-Newtonian Flow", Elsevier, Amsterdam, (1984).
55. Cressely R and Hocquart R, *Optica Acta*, 27 (1980) 699-711.
56. Mead D W, PhD Thesis, University of Cambridge, (1987).
57. Warichet V and Legat V, *J. Non-Newtonian Fluid Mech.*, 73 (1997) 95-114.
58. Luo X L, *J. Non-Newtonian Fluid Mech.*, 79 (1998) 57-75.
59. Baaijens F P T, Selen S H A, Paijens H P W, Peters G W M and Meijer H E H, *J. Non-Newtonian Fluid Mech.*, 68 (1997) 173-203.
60. Fan Y, Tanner R I and Phan-Thien N, *J. Non-Newtonian Fluid Mech.*, 84 (1999) 233-256.
61. Petera J, *J. Non-Newtonian Fluid Mech.*, 103 (2002) 1-43.
62. Fan Y, *J. Non-Newtonian Fluid Mech.*, 110 (2003) 77-102.
63. Sun J, Phan-Thien N and Tanner R I, *J. Non-Newtonian Fluid Mech.*, 65 (1996) 75-91.
64. Chauviere C and Owens R G, *J. Non-Newtonian Fluid Mech.*, 95 (2000) 1-33.
65. Harlen O G, *J. Non-Newtonian Fluid Mech.*, 37 (1990) 157-173.
66. Lunsman W L, Genieser L, Armstrong R C and Brown R A, *J. Non-Newtonian Fluid Mech.*, 48 (1993) 63-99.
67. Jin H, Phan-Thien N and Tanner R I, *Comp. Mech.*, 8 (1991) 409-422.
68. Khomami B, Talwar K K and Ganpule H K, *J. Rheol.*, 38 (1994) 255-283.
69. Fan Y and Crochet M J, *J. Non-Newtonian Fluid Mech.*, 57 (1995) 283-311.
70. Sigli D and Coutanceau M, *J. Non-Newtonian Fluid Mech.*, 2 (1997) 1-21.
71. Bisgaard C and Hassager O, *Rheol. Acta*, 21 (1982) 537-539.
72. Bisgaard C, *J. Non-Newtonian Fluid Mech.*, 12 (1983) 283-302.

73. Arigo M and McKinley G H, *Rheol. Acta*, 37 (1998) 307-327.
74. Maalouf A and Sigli D, *Rheol. Acta*, 23 (1984) 497-507.
75. Bush M B, *J. Non-Newtonian Fluid Mech.*, 55 (1994) 229-247.
76. Harlen O G, *J. Non-Newtonian Fluid Mech.*, 108 (2002) 411-430.
77. Satrape J V and Crochet M J, *J. Non-Newtonian Fluid Mech.*, 55 (1994) 91-111.
78. Harlen O G, Rallison J M and Szabo P, *J. Non-Newtonian Fluid Mech.*, 60 (1995) 81-104.
79. Cho Y I, Harnett J P and Lee W Y, *J. Non-Newtonian Fluid Mech.*, 15 (1985) 61-74.
80. Ambeskar V D and Mashelkar R A, *Rheol. Acta*, 29 (1990) 182-191.
81. Hassager O, *Nature*, 279 (1979) 402-403.
82. Astarita G and Apuzzo G, *AICHE J.*, 11 (1965) 815-820.
83. Zana E and Leal L G, *Int J Multiphase Flow*, 4 (1978) 237-262.
84. Leal L G, Skoog J and Acrivos A, *Can. J. Chem. Eng.*, 49 (1971) 569-575.
85. Liu Y J, Liao T Y and Joseph D D, *J. Fluid Mech.*, 304 (1995) 321-342.
86. Rodrigue D, De Kee D and Fong C F C M, *J. Non-Newtonian Fluid Mech.*, 79 (1998) 45-55.
87. Rodrigue D, De Kee D and Fong C F C M, *J. Non-Newtonian Fluid Mech.*, 66 (1996) 213-232.
88. Herrera J R, Zenit R, Chehata D and Mena B, *J. Non-Newtonian Fluid Mech.*, 111 (2003) 199-209.
89. Noh D S, Kang I S and Leal L G, *Phys. Fluids A*, 5 (1999) 1315-1332.
90. R. Zenit, D. Chehata and B. Mena, submitted to *J. Non-Newtonian Fluid Mech.*